Temperature of nonequilibrium steady-state systems

András Baranyai
Department of Theoretical Chemistry, Eötvös University, P.O. Box 32, 1518 Budapest 112, Hungary
(Received 10 April 2000)

We determined the *operational* temperatures of nonequilibrium-molecular-dynamics (NEMD) systems by the recently developed thermometer [A. Baranyai, Phys. Rev. E **61**, R3306 (2000)] and compared these values to the *dynamic* temperatures [H. H. Rough, Phys. Rev. Lett. **78**, 772 (1997)] of the same systems. NEMD models use a *synthetic thermostat*, a numerical feedback procedure to remove the dissipative heat instantaneously. A consequence of this feedback is a splitting of the dynamic temperature. The kinetic part is different from the configurational part because the energy is removed through the momentum subspace of the system. In addition to this, these temperature values also vary with respect to the direction of the external perturbation. In the case of planar Couette flow and color flow, the isotropic operational temperatures of dense liquids are always closer to the configurational than to the kinetic temperatures. We show that the observed split and the pronounced directional dependence of the dynamic temperature is an artifact caused by the instantaneous feedback of NEMD models. Since relaxation of a preset difference between the kinetic and the configurational temperature is an order of magnitude faster than the relaxation of the heat flux vector, for models with realistic thermostas such a split must be very small. We argue that in real systems, even far from equilibrium, the operational temperature and both terms of the dynamic temperature must be practically identical and isotropic.

PACS number(s): 05.70.Ln

I. INTRODUCTION

The thermodynamics of nonequilibrium states has always been a matter of debate. In the case of steady-state hydrodynamic systems atomistic computer simulation may be the way to answer at least some of the open questions. These type of studies, initiated and developed by Hoover, Evans, and co-workers [1,2], in addition to mimicking the behavior of real liquids, established connections between realistic models and the theory of nonlinear systems [3]. However, to formulate a theory of thermodynamic character proves to be difficult even for these models. While dynamic properties of the system are well-understood, thermodynamic variables such as temperature and entropy are still matters of controversy with questions even about their existence or usefulness for systems far from equilibrium [4].

The purpose of the present paper is to contribute some numerical data as ''experimental evidence'' to the understanding of nonequilibrium-steady-state (NESS) systems. The paper is focused on various concepts of temperature discussed in connection with nonequilibrium-molecular-dynamics (NEMD) simulations. The opportunity is provided by two recent developments. The *dynamic* concept of the temperature of Rugh [5] is based on the classical statistical mechanics of equilibrium systems and is readily obtained from computer simulations. The other is the *operational* thermometer of the present author [6]. So far only the kinetic (or equipartition) temperature was considered as *the* temperature, although it became obvious a decade ago that the concept of temperature in NEMD models appears to be more complicated than that [7].

The concept of the *dynamic* temperature is based on the classical statistical mechanics of equilibrium systems, so it is straightforward to calculate that in atomistic computer simulations. The dynamic temperature is a phase variable and not a functional of microscopic states. Its derivation utilizes the thermodynamic relationship. $T=(\partial U/\partial S)_{V,N}$, by expressing the entropy as the logarithm of the volume of the phase space [5],

$$\frac{1}{kT}=\left\langle \frac{\nabla\cdot\nabla H}{|\nabla H|^2}\right\rangle + o\left(\frac{1}{N}\right), \tag{1}$$

where H is the classical Hamiltonian of the system and the gradient operator is taken over the full phase space. The angular brackets denote a microcanonical average. Expressing Eq. (1) in a computationally more explicit form [neglecting the $o(1/N)$ term], we obtain [8]

$$\frac{1}{kT}=\frac{\left\langle \frac{dN}{m}+\nabla_r^2\Phi\right\rangle}{\left\langle \sum_{i=1}^{N}\frac{p_i^2}{m^2}+|\nabla_r\Phi|^2\right\rangle}=\frac{\frac{dN}{m}-\left\langle 2\sum_{i=1}^{N}\sum_{j>i}^{N}X_{ij}\right\rangle}{\left\langle \sum_{i=1}^{N}\frac{p_i^2}{m^2}\right\rangle+\left\langle \sum_{i=1}^{N}F_i^2\right\rangle}, \tag{2}$$

where k is Boltzmann's constant, m is the uniform mass of each of the N particles, d is the dimensionality of the system, $\Phi(\mathbf{r}_1,\mathbf{r}_2,\ldots,\mathbf{r}_V)$ is the potential energy, $\mathbf{p}_i$ and $\mathbf{F}_i$ are the momentum of and the Newtonian force on particle i, and $X_{ij}\equiv\nabla_{r_{ij}}\cdot\mathbf{F}_{ij}$. Averages both in the numerator and the denominator contain kinetic and configurational contributions. The ratio of only the first terms gives the well-known kinetic and the ratio of only the second terms gives the *configurational* temperature. In closed equilibrium systems these two temperatures are equal.

It is important to note that both the kinetic and the configurational temperatures have the correct dimensionality, but the dimensionality of the first and the second terms in the

complete expression is not the same [9]. If one eliminates this inconsistency by using dimensionless quantities, the choice of a set of reduction parameters will influence the relative weights of kinetic and configurational contributions. This is not a problem at equilibrium: we can define the two terms separately as the kinetic and the configurational temperatures of the system.

However, using this temperature concept in our special numerical experiments, we have to address the question of the correct reduction scheme, i.e., the unique partition of kinetic and configuration temperatures. In a recent paper, Ayton *et al.* [9] studied the validity of Fourier's law in systems with spatially varying strain rates. They constrained the two components, the kinetic and the configurational temperature, separately. Their results seemed to resolve a particular contradiction [10] if instead of the kinetic temperature the whole dynamic (they termed it as ''normal'') temperature was used [9].

Gradients of both temperature terms can generate a heat current. If the configurational and the kinetic temperatures differ, it might be important to know their contribution to the flow of energy. While there is no configurational contribution in infinite dilution, at finite density the configurational part becomes substantial. Adopting the usual reduction units of liquid state computer simulations, this part represents 95–99% of the total dynamic temperature for simple (Lennard-Jones-type) dense liquids [11]. We are not aware of any purely theoretical argument for a correct reduction scheme. It is not easy to provide a convincing numerical demonstration either, because of the fast equilibration of the two components of the dynamic temperature (see Sec. IV for more details). In the following, we provide our reduction scheme and present the kinetic and the configurational temperatures separately.

Evans and co-workers have shown that arbitrary phase-space vector fields can be used to generate phase functions whose ensemble average gives the dynamic temperature [8]. They also discussed numerical properties of the configurational temperature in molecular-dynamics simulations [8,12]. Recently, we showed that the dynamic temperature can be estimated in open regions too, because it follows from the condition of the time-independent temperature [13].

Since derivations of the dynamic temperature [5,8] rely on the formalism of equilibrium statistical mechanics, it is reasonable to have reservations about the applicability of this quantity to systems far from equilibrium. Clearly, to use this quantity for nonequilibrium problems is an extension based on analogy. One of the aims of this study is to support (or oppose) the use of the dynamical temperature away from equilibrium. The analogy must not be rejected out of hand because the relationship introduced in Ref. [13] connects the two parts of the dynamic temperature without making any reference to the equilibrium state of the system. If only Newton's laws govern the motion of particles and there is no correlation between velocities and configuration-dependent quantities for finite regions of the system, the kinetic and configurational temperatures are equal [13]. The results of Ayton *et al.* [9] are also encouraging in this respect.

The *operational* thermometer is a numerical measuring device, a piece of a solid crystal which has the shape and size of an ordinary particle in the dissipative fluid [6]. If the cohesive forces of the solid are strong enough, small particles of the thermometer crystal stay together as an almost equilibrium entity. The forces of the surroundings translate and rotate the thermometer as a whole and exchange heat with its random degrees of freedom. While the energy of the NEMD system is controlled by a numerical feedback mechanism to maintain a steady state, the temperature of the thermometer is free to choose its own value. After some initial period, the heat transferred from the dissipative fluid to the thermometer and back is equal and the resulting random kinetic energy of thermometer particles defines the *operational* temperature of the dissipative system [6].

There are several questions to be answered. What is the relationship between the operational and the dynamic temperature in thermostated NEMD models? What is the relationship between these two temperatures in more realistic nonequilibrium model calculations where the dissipative heat is conducted toward the boundaries by the system itself? The dynamic temperature is an equilibrium concept, but can it be generalized to nonequilibrium systems? In the following we try to find answers to these questions. Obviously, by numerical experiments we can provide no rigorous proofs but only numerical data. Nevertheless, the presented evidence shows a more coherent picture of the temperature for steady-state hydrodynamic systems far from equilibrium than we had so far. In Sec. II, we compare the dynamic and the operational temperature for NEMD models following the approach of our previous study [6]. In Sec. III, we present results for realistic models of nonequilibrium-steady-state systems. In Sec. IV, we discuss the causes of the pronounced split of the dynamic temperature in feedback-thermostated NEMD models. Finally, in Sec. V, we conclude this study.

II. DYNAMIC TEMPERATURE AND OPERATIONAL TEMPERATURE IN NEMD MODELS

We use the same system as in our previous paper [6]; details not presented in the following can be found there. We choose the SLLOD (so called because of its connection to Doll's tensor algorithm of Hoover [1]) and the color conductivity algorithms as NEMD models [2]. The former method (apart from the synthetic thermostat) is an exact realization of planar Couette flow. It is valid well beyond the linear regime, as long as the linear velocity profile is stable. Its equations of motion are as follows:

$$\dot{\mathbf{q}}_i = \frac{\mathbf{p}_i}{m_i} + \mathbf{e}_x \gamma y_i ,$$

$$\dot{\mathbf{p}}_i = \mathbf{F}_i - \mathbf{e}_x \gamma p_{yi} - \alpha \mathbf{p}_i , \tag{3}$$

where $\mathbf{e}_x$ is a unit vector. The constant shear rate is defined as $\gamma \equiv \partial u_x / \partial y$ and α is the thermostating multiplier given by the Nosé-Hoover integral feedback formula [1]. Equation (3) describes the motion of the fluid particles. In the case of the particles of the thermometer, there is no thermostat, i.e., the last term of the momentum equation of Eq. (3) is missing. A further difference is that the streaming terms [the second terms on the right-hand side of Eq. (3)] act on the particles via the motion of the crystal's center of mass [6].

TABLE I. Results for shear flow. $T_{K\alpha}$ is the kinetic temperature of direction α; $T_{C\alpha}$ is the configurational temperature of direction α; $T_O(m_s=0.2)$ is the operational temperature with thermometer particle mass of 0.2 Asterisks refer to the thermometer size of 321 particles.

Shear rate	0.1	0.2	0.3	0.4	0.5
T_{Kx}	1.013(3)	1.032(5)	1.046(5)	1.024(4)	0.927(10)
T_{Ky}	0.997(2)	1.008(3)	1.032(3)	1.098(3)	1.219(10)
T_{Kz}	0.982(3)	0.954(4)	0.918(4)	0.873(3)	0.848(8)
T_{Cx}	1.011(5)	1.052(3)	1.103(4)	1.145(4)	1.189(5)
T_{Cy}	1.005(4)	1.055(3)	1.142(4)	1.296(5)	1.566(8)
T_{Cz}	0.983(4)	0.970(5)	0.964(4)	0.971(5)	1.017(6)
$T_O(m_s=0.2)$	1.02(2)	1.10(4)	1.16(4)	1.33(5)	1.45(5)
$T_O(m_s=1.0)$	1.01(2)	1.06(4)	1.18(4)	1.23(5)	1.40(7)
$T_O(m_s=0.2)$*	1.01(2)	1.11(4)	1.23(5)	1.27(6)	1.50(7)
$T_O(m_s=1.0)$*	1.01(2)	1.06(4)	1.19(4)	1.25(6)	1.42(7)

The color flow algorithm is similar to the model of a 1-1 molten salt under the impact of a constant electric field. The equations of motion are [2]

$$\dot{\mathbf{q}}_i=\frac{\mathbf{p}_i}{m},$$
$$\dot{\mathbf{p}}_i=\mathbf{F}_i+\mathbf{e}_x\mathbf{c}_iF-\alpha(\mathbf{p}_i-\mathbf{e}_xc_iJ), \tag{4}$$

where $c_i\equiv(-1)^i$ is the color charge of particle i. The color field and the color current are F and $J\equiv 1/N\Sigma_{i=1}^{N}c_i\dot{x}_i$, respectively.

Both models represent anisotropic systems. Even their kinetic temperatures show strong directional dependence: $T_{Kx}\equiv 1/[(N-C/3)k]\Sigma_{i=1}^{N}(p_{ix}^2/m_i)$ is different from the analogously defined T_{Ky} or T_{Kz}. (The number of constraints in the system is C.) Typically the smallest of them is T_{Kz}, which is the direction perpendicular to the shear plane. In the case of color conductivity, the anisotropy is less pronounced. The largest value, T_{Kx}, belongs to the direction of the flow. (Note that in the latter case, the x momentum, reduced by its systematic part, is used for temperature determination.)

The configurational temperature can also be defined for different directions. This quantity along the x direction can be written in a computationally explicit form,

$$\frac{1}{kT_{Cx}}=\frac{\left\langle 2\sum_{i=1}^{N}\sum_{j>i}^{N}X_{ij}\right\rangle}{\left\langle\sum_{i=1}^{N}F_{ix}^2\right\rangle}, \tag{5}$$

where $X_{ij}\equiv dF_{ijx}/[d(x_j-x_i)]$. The particular task of the following calculation is to estimate the T_C components for a fixed kinetic temperature, $T_K=(T_{Kx}+T_{Ky}+T_{Kz})/3.0$, and to measure the isotropic operational temperature, T_O, simultaneously.

We studied the same systems as in our previous paper [6], in order to provide an opportunity for the reader to look at other properties of the models. Every numerical details of the calculations was the same (interactions, units, run lengths, etc.). Here, only the temperature values determined by the three different methods are shown.

The shear-flow results are presented in Table I. Due to its definition, the operational temperature is isotropic. In the middle of the crystal, the kinetic temperature is higher by 0.1–0.4 % than its value for the entire crystal. The same behavior can be observed in the case of the configurational temperature of the crystal, which, in most cases, is higher by 0.5–1.0 % than its kinetic counterpart. Both the kinetic and the configurational temperatures of the dissipative fluid are anisotropic and can be calculated by an order of magnitude more accurately than the operational temperature. This is reasonable because the temperature of the thermometer is set only via collisions, while, at every instant, the complete dynamics of the whole fluid determines its kinetic or configurational temperatures. The relaxation time of the operational thermometer in the studied systems is several hundred time units, depending on the mass of the thermometer particles, the strength of the external field, etc. The operational temperatures are even less certain in the case of the high shear rate simulations (0.4 and 0.5). These systems are more or less in the ''string'' phase, which can maintain particular dynamics for long periods of the simulation depending on the history of their preparation.

The anisotropy of the kinetic temperature becomes more pronounced with increasing shear rate. (The sum of the components is constrained for 3.0). The z component of the kinetic temperature shows a monotonic decrease with the shear rate. For small shear rates, the y component is smaller than the x component. However, for very high shear rates, when the dynamics becomes ''stringlike,'' the y component is the largest one. The configurational temperature follows this general trend but the calculated values are always larger than the corresponding kinetic ones. The differences are substantial, well beyond the uncertainties of the calculations. Interestingly, the configurational y component, with the exception of the smallest shear rate, is larger than the corresponding x component.

We tested two masses for thermometer particles (0.2 and 1.0) and two sizes for thermometers (135 and 321 particles). Internal properties of the thermometer crystal exerted only a negligible influence on the properties of the fluid. Thus, fluid temperatures with different thermometers are not shown separately. Despite the uncertainties, as we pointed out in our previous paper [6], the operational temperatures are significantly larger than the corresponding kinetic temperatures of

TABLE II. Results for color flow. For the definition of symbols, see Table I.

Color field	0.0	0.5	1.0
T_{Kx}	1.000(2)	1.023(2)	1.180(5)
T_{Ky}	1.000(2)	0.989(2)	0.923(6)
T_{Cx}	1.000(2)	0.994(3)	0.940(8)
T_{Cy}	1.000(2)	0.988(4)	0.912(6)
$T_O(m_s=0.2)$	1.00(2)	0.99(2)	0.94(3)
$T_O(m_s=1.0)$	1.00(2)	0.99(3)	0.92(3)
$T_O(m_s=0.2)$*	1.00(2)	0.99(2)	0.93(3)
$T_O(m_s=1.0)$*	1.00(2)	0.99(2)	0.94(3)

the fluid. The y component of the configurational temperature of the dissipative fluid seems to be the closest one to the corresponding operational temperature.

We present temperature values of color conductivity calculations in Table II. In contrast to shear flow, the configurational temperature is smaller than the corresponding kinetic one. Both the kinetic and the configurational temperatures are higher in the direction of the flow (parallel to the x axis) than in perpendicular directions. The operational temperature is very close to the configurational temperature, it is only the x component of the kinetic energy that is substantially different from the other temperatures.

It would be interesting to establish a unique connection between the dynamic and the operational temperature. Obviously, it is the whole dynamics of the dissipative fluid which determines the value of the latter. However, there are several uncertainties that are difficult, or even impossible, to clarify in such a calculation. The operational temperature is not a perfectly universal quantity because the energy of the crystal (kinetic and configuration-dependent) is a function of the thermal conductivity of the thermometer-fluid boundary. To maintain homogeneity, the thermometer must behave like one of the fluid particles, so properties of the boundary region of the thermometer (including thermal conductivity) might be slightly different for different particle interactions. Nevertheless, we doubt that discrepancies originating from this, at least for simple models used in these calculations, can be large enough to be detectable. From the point of view of numerical accuracy, ensuring the ergodic sampling of collisions is more important. To obtain reliable estimates for operational temperature values, much longer calculations would be necessary. Still, this could not establish a unique connection between the two concepts of the temperature. Contributions to the dissipative energy flux from the kinetic and the configurational temperatures must be partitioned unambiguously. As we alluded to this problem in the Introduction, this is not a trivial task.

III. DYNAMIC TEMPERATURE IN NESS MODEL SYSTEMS WITHOUT A SYNTHETIC THERMOSTAT

It is obvious that measuring the operational temperature of *inhomogeneous* nonequilibrium systems is problematic, even in a steady state. It takes some time for the crystal and the liquid to come to thermal balance. (The relaxation time of the thermometer is about 10^5-10^6 time steps.) During this time, however, the thermometer crystal might diffuse away into a region where properties, including the ones determining the operational temperature, are different. Fixing the relative position of the thermometer and a given region of the inhomogeneous liquid by some numerical constraint will distort the results. Thus, for inhomogeneous NESS models, we compared only the kinetic and configurational temperatures.

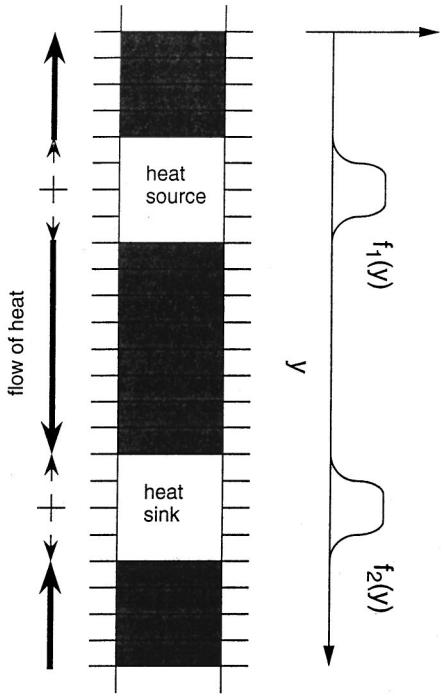

FIG. 1. A two-dimensional projection of the scheme representing the simulation cell of heat-flow calculation. (See text for details.)

Two types of model systems were used. Both can be considered as realistic models, in the sense that no synthetic thermostat is applied. As a result, these fluids are inhomogeneous. The first model applies the heat conductivity algorithm of the present author [14]. This method is a modern version of early ''naive'' attempts [15] before the synthetic algorithm of Evans was derived [16]. Since we simplified the original algorithm of Ref. [14], it is useful to give a short description of the method.

In Fig. 1, we show a two-dimensional schematic projection of our simulation box. The system has translational periodicity in every direction. The hot and cold regions which are represented by white squares are under the impact of synthetic thermostats. In the dark areas, only Newton's equations govern the motion of particles. The fluid system is continuous: particles can wander in and out of each part of the elongated simulation box. We do not interfere with this motion because the positions of particles determine whether they belong to a reservoir or to the Newtonian (thermostat-free) region. To avoid discontinuity at reservoir boundaries, we apply a continuous spatial switch-on function to mark the thermostat particles. In the present simulation, the form of this function is $f(y')=y'^4-2y'^2+1$, where $y'=2(y/l_y-0.5)$ or $y'=2[(y-L_y/2)/l_y-0.5]$ and L_y and l_y are, respectively, the box length and the length of the reservoir region in the y direction. The equations of motion are

$$\dot{\mathbf{q}}_i = \mathbf{p}_i/m,$$
$$\dot{\mathbf{p}}_i = \mathbf{F}_i - f_\beta(y_i)\alpha_\beta \mathbf{p}_i, \tag{6}$$

where the subscript $\beta=1,2$ distinguishes between hot and cold parts of the system. The two functions have identical shapes but the first is different from zero only in the hot reservoir, while the second is different from zero only in the cold reservoir. The x component of the kinetic temperature of the reservoir is defined as follows:

$$T_{x\beta} = \frac{\sum_{i=1}^{N} f_\beta(y_i) p_{ix}^2}{km \sum_{i=1}^{N} f_\beta(y_i)}. \tag{7}$$

The time derivative of $T_\beta = (T_{x\beta} + T_{y\beta} + T_{z\beta})/3.0$ is constrained to zero during the simulation. This differential feedback and the total momentum of reservoir regions are corrected by a continuous feedback during the course of simulations [17]. In steady state, the energy input and output are identical and can be given as

$$\dot{Q}_\beta = -\alpha_\beta \sum_{i=1}^{N} \frac{\mathbf{p}_i^2}{m} f_\beta(y_i). \tag{8}$$

The heat conductivity can be calculated using the constitutive relation of $J_y = -\lambda dT/dy$, where $dT/dy = (T_{\text{hot}} - T_{\text{cold}})/L_y$ and $J_y = \dot{Q}_{\text{in}}/2L_xL_z$. Due to the requirement of translational periodicity, the reservoirs are connected by two Newtonian regimes. (See Fig. 1.) This is the reason for the factor of 2 in the denominator of the heat flux. In the limit of the infinitely thin reservoir ($l_y \to 0$), the dynamics of our system is determined entirely by Newton's equation of motion. In this limit, zero-field heat conductivity calculated by the formulas above gives values identical with those of the synthetic method of Evans [11].

Adopting the same approach we devised a model for shear flow. The reservoir regions were given an additional role, an external field acted and accelerated the particles. The form of the spatial switch-on function was identical with that of the heat-flow algorithm above. A similar method was used in one of our earlier works [18]. The momentum equation of motion is

$$\dot{\mathbf{p}}_i = \mathbf{F}_i - f_\beta(y_i)(\mathbf{e}_x F_\beta + \alpha_\beta \mathbf{p}_i), \tag{9}$$

where $F_1 = -F_2$. A difference between the heat-flow and the shear-flow algorithms is that, for the sake of simplicity, the temperature control is carried out by an integral feedback in the latter case.

To model particle interactions, we used a simple soft-core potential defined as follows:

$$\phi(r) = \begin{cases} 4[r^{-12} + r^{-6}] + 1, & r < 2^{1/6}, \\ 0, & r > 2^{1/6}. \end{cases}$$

In the calculations, we applied the usual reduced units of computer simulations [19]. The length of the simulations was several thousand reduced time units, depending on the size of the system with a time step of 0.002. The equations of motion were integrated by a fifth-order Gear integrator for a fluid density 0.8. The average temperature was 1.0.

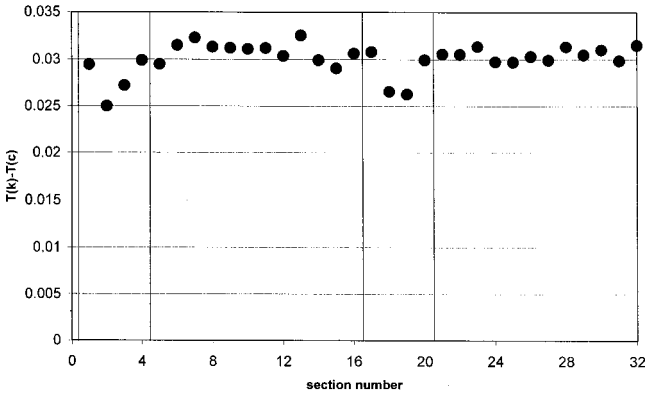

FIG. 2. Difference between the kinetic, $T(k)$, and the configurational, $T(c)$, temperatures as determined for different sections of the equilibrium fluid. The vertical bars mark the thermostated regions. The system is periodic. (Number of particles is 864, number density is 0.8, kinetic temperature is 1.0, both in reduced units.)

The numerical results of Evans and co-workers showed a non-negligible system-size dependence of the configurational temperature for closed systems [8,12]. This might be even more important for small open regions of the system [13]. The configurational temperature might be systematically different from the corresponding local average of the kinetic temperature. In the case of heat flow, to study this behavior, we performed simulations for different system sizes. Aligning eight identical cubes along the y axis, we had 864(8×108), 2048(8×256), and 4000(8×500) particles. The simulated fluid was divided up into 32 sections along the y direction. (See Fig. 1.) Each section (or slice of fluid) represented a local environment within which the averages were collected. We also performed equilibrium simulations for each system size, which served as references to show the difference between local kinetic and local configurational temperatures at equilibrium.

In Fig. 2, we show this difference in an equilibrium system consisting of 864 particles. The temperature of the system was fixed to 1.0 by using the feedback thermostat of Eq. (6). In sections 1–4 and 17–20, where the thermostat acted by adding or removing random kinetic energy, the difference between the kinetic and the configurational temperature is slightly smaller than in the rest of the fluid. The average difference in the thermostat-free regions is 0.031. This value in the systems of 2048 or 4000 particles is considerably smaller, 0.014 and 0.009, respectively. Thus, as one might expect, the two types of temperatures become identical in the thermodynamic limit.

To see the impact of a nonequilibrium flow, we fixed the two thermostats (in sections 1–4 and 17–20) to different but constant temperatures. For the system of 864 particles, the temperatures were 0.85 and 1.15; for the system of 2048 particles, they were 0.80 and 1.20; while for the system of 4000 particles, these values were 0.75 and 1.25. This way we introduced identical temperature gradients to each of the three systems with identical temperature (1.0) in the middle of the Newtonian region. However, the sizes of the sections distinguished by temperature averaging were different. In

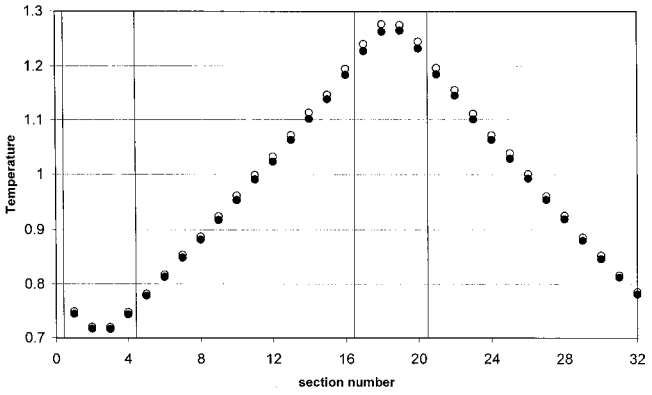

FIG. 3. Temperature distribution of the heat-flow model. Dark circle, configurational temperature; open circle, kinetic temperature. The vertical bars mark the thermostated regions. The system is periodic. (Number of particles is 4000, average number density is 0.8 in reduced units.)

Fig. 3 we present the temperature distribution of the largest system (4000 particles). The temperature gradient outside of the reservoir regions (between 5 and 16 or 21 and 32) is practically uniform. (To study other properties of this heat-flow model system, the reader is referred to Ref. [14].) In Fig. 4, we present the differences between the kinetic and the configurational temperature values for the three system sizes. Exploiting the symmetry of the systems, we averaged the physically equivalent sections (5–32, 6–31, etc.) and show only the left-hand side of the previous diagram. We found a behavior similar to what we had in the equilibrium case: the difference between the kinetic and the configurational temperatures seemed to diminish with increasing section size. This is the case around section 11, too, where not only the temperature gradient but also the kinetic temperature and the number density were identical in the three systems. (Both the temperature and the number density of this model change practically linearly with distance along the direction of the heat flow [14].) Since the functions of Fig. 4 are not constants, properties of nonequilibrium systems influence the

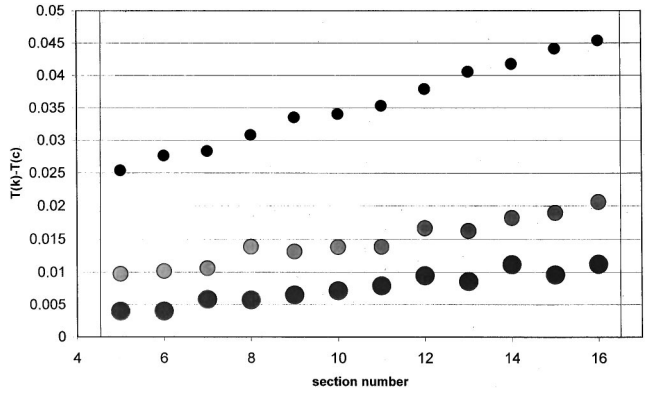

FIG. 4. Difference between the kinetic, $T(k)$, and the configurational, $T(c)$, temperatures. Small circle, system of 864 particles; medium-sized circle, system of 2048 particles; large circle, system of 4000 particles. Utilizing the periodicity of the system, equivalent sections were averaged. Sections where the thermostat is on are not shown. (Average number density is 0.8, temperature gradient is 0.014 62, medium temperature is 1.0. All are given in reduced units.)

difference between the two temperature definitions. However, it is obvious from the diagram that the impact of this influence goes to zero if larger and larger slices of the fluid are used for calculating averages. In the thermodynamic limit, nonequilibrium properties do not seem to influence the split of the dynamic temperature.

It should be noted that Eqs. (6)–(9) fixed only the kinetic temperature, which might show these results to be less convincing. Unfortunately, constraining the configurational temperature numerically is very complicated. However, differences of the kinetic and configurational temperature in the thermostated regions are very similar to values found elsewhere in the system. At the end of the following section, it will become clear that this is not accidental: it is the result of the fast relaxation of the dynamic temperature split. This renders the configurational temperature constraint unnecessary.

Although temperature gradients and accompanying density and internal energy variations were enormous, properties of the heat-flow model vary practically linearly with distance along the direction of the heat flow. Someone might argue that the extrapolated equivalence of the kinetic and the configurational temperature is the result of this linearity, as if our model liquids were in the linear regime. In the case of the shearing liquid model, however, this is obviously not the case. System properties manifest the far-from-equilibrium character of the model. To demonstrate this, we present several properties of this model. To the best of our knowledge, this is the first application of this algorithm. Our system had 864 or 2048 particles with the same average density, 0.8. The thermostats constrained the reservoir temperatures to 1.0 and, at the same time, a fictitious force accelerated the fluid particles in this region. (Contrary to the heat-flow case, it is impossible to create identical models with different sizes. The viscous heat generated by the same shear rate has to travel a longer distance before reaching the reservoirs in the larger system. Therefore, the temperature profile of the larger system with identical shear rate shows higher temperatures than that of its small-system counterpart.) We divided up every shearing system into 64 sections to have good resolutions. Sections 1–6 and 33–38 represented the reservoirs.

We studied the impact of system sizes at two shear rates: 0.139 and 0.066. In Fig. 5, the streaming velocity of different fluid sections is shown, together with the kinetic temperature in the x direction for the system of 2048 particles. To obtain local temperatures, particle velocities should be reduced with the average local streaming velocities. This has been done for all three directions, although it was only the x direction that had large and systematic streaming velocities, as shown in Fig. 5. (The kinetic temperature values presented in Fig. 5 were calculated without reduction by streaming.) We present the shear rate and the shear stress in Fig. 6 for the same system. The shear rates were calculated using simply the differences of streaming velocities between neighboring sections. The uniformity of the shear stress demonstrates the accuracy of the method.

In Fig. 7, we compare the temperatures of systems of 2048 particles with two different shear rates: 0.139 and 0.066. We show the configurational and kinetic values separately. In the case of the high shear rate, the viscous heating creates much larger temperatures in the middle of the New-

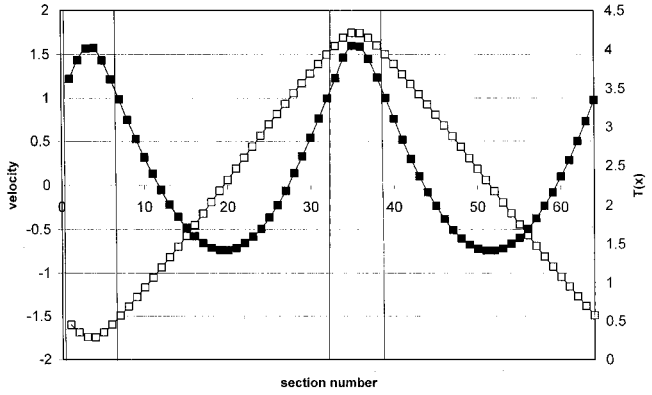

FIG. 5. Average velocity (open squares) and the x component of the kinetic temperature, $T(x)$, calculated (dark squares) in the shearing system of 2048 particles. The streaming contribution has not been removed from $T(x)$. Vertical bars mark the thermostated regions. (Average number density is 0.8, $F_\beta = \pm 0.1$. Both are given in reduced units.)

tonian region where no synthetic thermostat is acting. The viscous heat travels towards the thermostats where the feedback keeps the temperature at 1.0. It is interesting to note that contrary to the heat-flow case, the configurational temperature is larger than the kinetic one.

While for the heat-flow model components of both the kinetic and configurational temperatures were practically identical, this is not the case for the shear-flow model. The kinetic temperatures are very close to one another again but configurational temperature in the y direction is larger than the roughly equivalent configurational temperatures in the x and z directions. (This was also the case in high-shear-rate NEMD models of the preceding section.)

We studied this behavior. The question is the same again: can nonequilibrium conditions maintain finite-temperature differences between components of configurational and kinetic temperatures? We performed simulations for both system sizes (864 or 2048 particles) with shear rates of 0.139 and 0.066, respectively. The configurational temperature was found to be larger than the corresponding kinetic one. In the case of the system of 864 particles, $T_C - T_K = 0.025$ for the x and z components and 0.043 for the y component. In the Newtonian region, these values do not vary with section

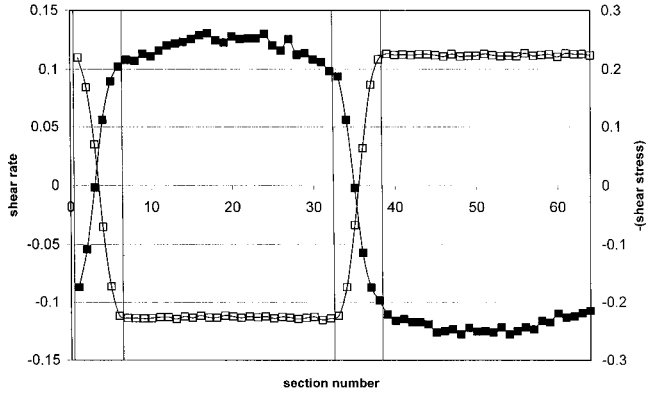

FIG. 6. The shear rate (dark squares) and the shear stress, $-P_{xy}$ (open squares), for the system of the preceding figure. Vertical bars mark the thermostated regions.

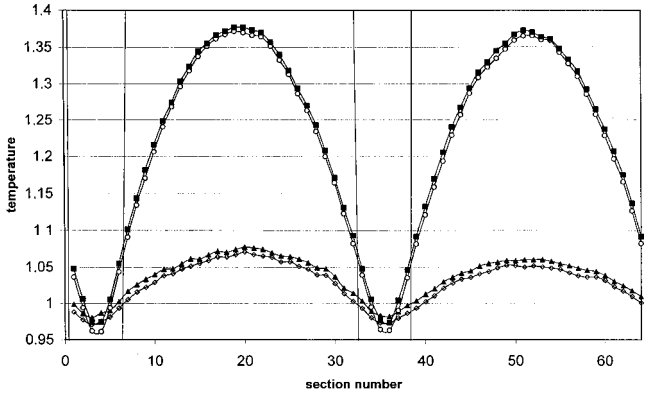

FIG. 7. Profile of the reduced kinetic and configurational temperatures for the system of 2048 particles. Dark squares, configurational temperature for $F_\beta = \pm 0.2$; open circles, reduced kinetic temperatures for $F_\beta = \pm 0.2$; dark triangles, configurational temperature for $F_\beta = \pm 0.1$; open diamonds, reduced kinetic temperatures for $F_\beta = \pm 0.1$. Vertical bars mark the thermostated regions. The system is periodic.

number. The splits are constant within the accuracy of the calculations. In this respect, it is more surprising that the differences are independent of the strength of the external field. These temperature differences were determined for both shear rates.

In the case of the larger system, the temperature differences are 0.006 for the x and z components and 0.013 for the y component. Although data for the larger system are less accurate, the behavior found in the smaller system is the same. The impact of the nonequilibrium field is marginal. The split is overwhelmingly a section-size effect. Larger sections produced smaller temperature differences. We performed additional calculations to check this behavior but the trend was found to be the same.

In light of these results, it is reasonable to expect that differences between the configurational and the kinetic temperatures, as well as differences between components of these, would disappear in the thermodynamic limit. This is not the case in NEMD models. Although configurational temperatures have a slight number dependence in these calculations, too, this does not diminish the temperature anisotropy and differences between the configurational and the kinetic temperatures.

In the preceding section, we could not relate the six different dynamic temperature components to the operational temperature. It was obvious that their relationship is not a trivial matter. In the case of realistic models, however, the practical equivalence of the kinetic and the configurational temperature components is very tempting. We could not measure the operational temperature, but it would be absurd to expect a value for this quantity different from the equivalent six dynamic temperature terms. In these systems, the local pattern of collisions is close to that of an equilibrium liquid.

IV. RELAXATION OF THE DYNAMIC TEMPERATURE

In the NEMD models of Sec. II, we experienced a significant difference between kinetic and configurational temperatures. For very large systems, these differences are expected

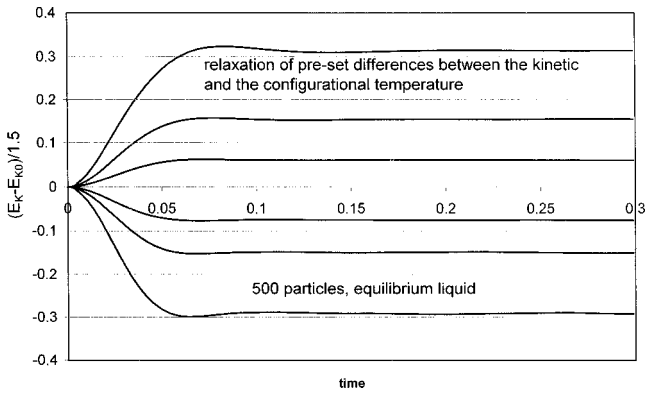

FIG. 8. Relaxation of the kinetic temperature to equilibrium. The curves from the top to the bottom show the relaxation after the starting kinetic temperature was set instantaneously to 0.0, 0.45, 0.72, 1.125, 1.35, and 1.8. (Number of particles is 500, reduced density is 0.8, reduced temperature is 0.9.)

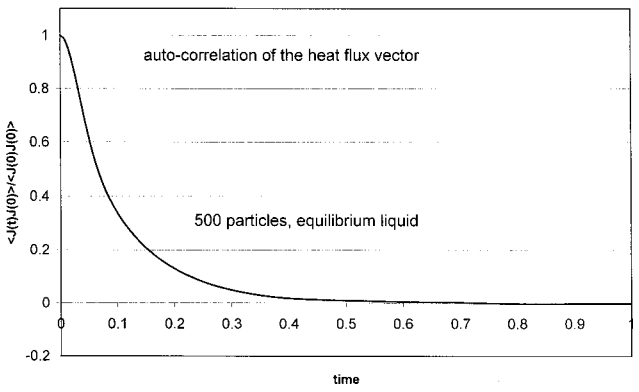

FIG. 9. Normalized autocorrelation of the heat flux vector. (Number of particles is 500, reduced density is 0.8, reduced temperature is 0.9.)

to disappear in the more realistic simulations shown in the preceding section. A pronounced decrease of anisotropy of the temperature is expected. Despite the anisotropy of naive models, the temperature seemed to behave like the temperature of an equilibrium system. The overwhelming drive towards randomness seems to ensure the zeroth law of thermodynamics, even in these anisotropic nonequilibrium fluids. Why is it not so in NEMD models with synthetic thermostats? The reason for this is quite simple, as we will see in the following numerical demonstration.

The regression hypothesis of Onsager claims that in the linear regime, when the system relaxes to its stable equilibrium state, one is unable to tell whether it was out of equilibrium due to spontaneous internal fluctuations or it was moved out of it by external perturbations. Utilizing this principle, we compared the relaxation of the dynamic temperature with the relaxation of the heat-flow vector.

We performed an equilibrium MD simulation and calculated the autocorrelation function of the heat-flow vector. We had 500 particles at the reduced density of 0.8 and temperature of 0.9. We used the same interaction model as in Sec. III. At the same state point, following the equilibrium trajectory of the same system, we created starting states after every 50 time steps (0.1 reduced time units) by artificially splitting up the dynamic temperature. We rescaled particle velocities instantaneously and in a nonequilibrium run calculated the relaxation of the system to equilibrium. Several thousand nonequilibrium trajectories were sufficient to see the average relaxation of the temperature split. In Fig. 8, we compare the results of the calculations. The *y* axis of the figure shows the reduced and scaled kinetic energy, which is defined as $(E_K - E_{K0})/1.5$. The curves from the top to the bottom show the relaxation after the starting kinetic temperature was set instantaneously to 0.0, 0.45, 0.72, 1.125, 1.35, and 1.8. Although these differences are extreme, the relaxation is very fast.

The normalized autocorrelation function of the heat flux vector is shown in Fig. 9. Relaxation of the dynamic temperature is an order of magnitude faster than relaxation of the heat-flow vector in the same system. *Temperature relaxation is a local, one-particle phenomenon*: if a particle has a large kinetic energy, it climbs up on the map of the potential energy and within a few time steps the statistical equilibrium between the kinetic and the configurational part of the temperature is established. In contrast, relaxation of the heat-flow vector is slower because it is a collective phenomenon.

Although the numerical evidence presented above is far from being exhausting, we believe, the relative speed of these relaxation processes must be similar in other models or real systems, too. Thus, in realistic far-from-equilibrium hydrodynamic models with natural conduction of the dissipative heat, a large split of the kinetic and the configurational temperature seems very unlikely. In realistic models and, as a matter of fact, in real systems, the speed of heat conduction is finite and slow compared to the local equilibration of the kinetic and the configurational temperature. It is the instantaneous, infinitely fast heat removal of NEMD models that is able to split up and stabilize the kinetic and the configurational parts of the dynamic temperature. In this respect the response time (the fictive mass) of the Nosé-Hoover scheme plays no role. There is a certain amount of average dissipative energy determined by the parameters of the model to be removed in each time step. The memory of the feedback cannot influence the value of this long-time average. Our test calculations confirmed this: the fictive mass of the thermostat had no impact on the splitting.

The dissipative energy is removed through the random momenta of the particles. There is no time for the configurations to follow this instantaneous process. Thus, *the configurational temperature* (with the possible exception of artificial regimes) *will be larger in NEMD models than the corresponding kinetic one.*

V. CONCLUSIONS

We performed various numerical experiments to study the concept of temperature in steady-state systems far from equilibrium. We simulated hydrodynamic models using both the homogeneous NEMD technology (SLLOD and color flow) with a synthetic thermostat and the so-called ''naive'' approach for heat flow and shear flow [14]. Besides the usual and trivial kinetic (or equipartition) temperature, the configuration-dependent part of the dynamic temperature of Rugh [5] and the operational temperature of the present author [6] were determined. The results showed a significant difference between the kinetic and configurational tempera-

tures of NEMD models. The latter was significantly larger in the case of shear flow and smaller in the case of the ''string phase'' of color flow. Both temperature contributions for both models were highly anisotropic. The corresponding operational temperatures were much closer to the configurational temperature values. The operational temperature is established through the incessant collisions of fluid particles with the thermometer. Features of these collisions are functions of the complete dynamics of the dissipative fluid. In dense fluids, it is the configurational part of the temperature which is important, although the exact relationship between the operational and the dynamic temperature cannot be determined.

The behavior of our realistic models (also far from equilibrium) was substantially different from that of NEMD systems. Our model fluids, mimicking heat flow and shear flow, contained only a limited region where feedback thermostats or external forces were acting. Due to their inhomogeneity, we had to study their properties locally. We experienced directional split and also differences between configurational and kinetic temperatures. However, these differences seemed to diminish with increasing systems. We found the impact of the nonequilibrium dynamics marginal compared with the size dependence of fluid element averages.

NEMD systems use a feedback procedure which removes the dissipative heat instantaneously. This energy control is carried out through the momentum subspace of the dynamics. Although equilibration of the configurational and kinetic part of the temperature is very fast, its speed is finite. Thus, in NEMD models the kinetic temperature is, in general, different from the configurational one.

The situation is the opposite in realistic models because the heat conduction of the system is much slower than the equilibration of the dynamic temperature. Still, hydrodynamic NESS systems are anisotropic. Using only numerical calculations, we cannot exclude the presence of this anisotropy in the temperature. However, in the thermodynamic limit, especially at realistic gradients and inhomogeinities, it seems unlikely that we can detect deviations from the isotropic temperature value.

Our results support the use of the concept of dynamic temperature for systems far from equilibrium. At least, the calculations did not point to any systematic problem with respect to this approach. We think the temperature in general is still a useful concept for steady-state hydrodynamic systems far from equilibrium.

The need for NEMD calculations in the 1970s was motivated by limited computer resources. To have a well-defined system, good signal/noise ratio, large external fields, and homogeneous models with synthetic thermostats were necessary. It must be pointed out that up-to-date computer power does not help to overcome the inherent problems of NEMD techniques. No matter how small the external field is, these models are correct only in the zero-field limit. Of course, there is no question about the usefulness of NEMD models. Results such as the conjugate pairing rule [20] or the fluctuation theorem [21] are proof of the importance of this approach. However, it must be kept in mind that outside the linear regime, these models have dynamics very different from that of real systems. They are not the ideal limiting cases of reality, like the ideal gas, but artificial models. They must be used with extreme care when details of real systems or experimental phenomena are to be understood. This is especially true when thermodynamics of nonequilibrium steady-state systems is concerned.

ACKNOWLEDGMENTS

The author gratefully acknowledges the support of OTKA through Grant No. T032481 and the support of the NSF-MTA Collaborative Research Program through Grant No. INT-9603005. Comments from Professor Bill Hoover and Dr. László Pusztai were very helpful.

[1] Wm. G. Hoover, *Computational Statistical Mechanics* (Elsevier, Amsterdam, 1991); *Time Reversibility, Computer Simulation and Chaos* (World Scientific, Singapore, 1999).
[2] D. J. Evans and G. P. Morriss, *Statistical Mechanics of Nonequilibrium Liquids* (Academic, London, 1990).
[3] D. Ruelle, *Thermodynamic Formalism* (Addison-Wesley, Reading, MA, 1978); G. Gallavotti and E. G. D. Cohen, Phys. Rev. Lett. **74**, 2694 (1995); P. Gaspard and J. R. Dorfman, Phys. Rev. E **52**, 3525 (1995).
[4] See, for instance, D. Jou and J. Casas-Vázquez, Phys. Rev. A **45**, 8371 (1992); Wm. G. Hoover, B. L. Holian, and H. A. Posch, *ibid.* **48**, 3196 (1993); K. Henjes, *ibid.* **48**, 3199 (1993); D. Jou and J. Casas-Vázquez, *ibid.* **48**, 3201 (1999).
[5] H. H. Rugh, Phys. Rev. Lett. **78**, 72 (1997).
[6] A. Baranyai, Phys. Rev. E **61**, 3306 (2000).
[7] D. J. Evans, J. Stat. Phys. **57**, 745 (1989); A. Baranyai and D. J. Evans, Mol. Phys. **74**, 353 (1991).
[8] O. G. Jepps, G. Ayton, and D. J. Evans, Los Alamos National Laboratory Print Archive, http://www.lanl.gov/abs/cond-mat/9906423.
[9] G. Ayton, O. G. Jepps, and D. J. Evans, Mol. Phys. **96**, 915 (1999).
[10] A. Baranyai, D. J. Evans, and P. J. Daivis, Phys. Rev. A **46**, 7593 (1992).
[11] A. Baranyai (unpublished).
[12] B. D. Butler, G. Ayton, O. G. Jepps, and D. J. Evans, J. Chem. Phys. **109**, 6519 (1998).
[13] A. Baranyai, J. Chem. Phys. **112**, 3964 (2000).
[14] A. Baranyai, Phys. Rev. E **54**, 6911 (1996).
[15] W. T. Ashurst, in *Advances in Thermal Conductivity* (University of Missouri–Rolla, Rolla, 1976); A. Tenenbaum, G. Ciccotti, and R. Gallico, Phys. Rev. A **25**, 2778 (1982).
[16] D. J. Evans, Phys. Lett. **91A**, 457 (1982).
[17] A. Baranyai and D. J. Evans, Mol. Phys. **70**, 53 (1990).
[18] A. Baranyai and P. T. Cummings, Mol. Phys. **90**, 35 (1997).
[19] M. P. Allen and D. J. Tildesley, *Computer Simulation of Liquids* (Clarendon, Oxford, 1987).
[20] D. J. Evans, E. G. D. Cohen, and G. P. Morriss, Phys. Rev. A **42**, 5990 (1990).
[21] D. J. Evans, E. G. D. Cohen, and G. P. Morris, Phys. Rev. Lett. **71**, 2401 (1993).